Joule

CellPress

Article

Over 15% efficient wide-band-gap $Cu(In,Ga)S_2$ solar cell: Suppressing bulk and interface recombination through composition engineering

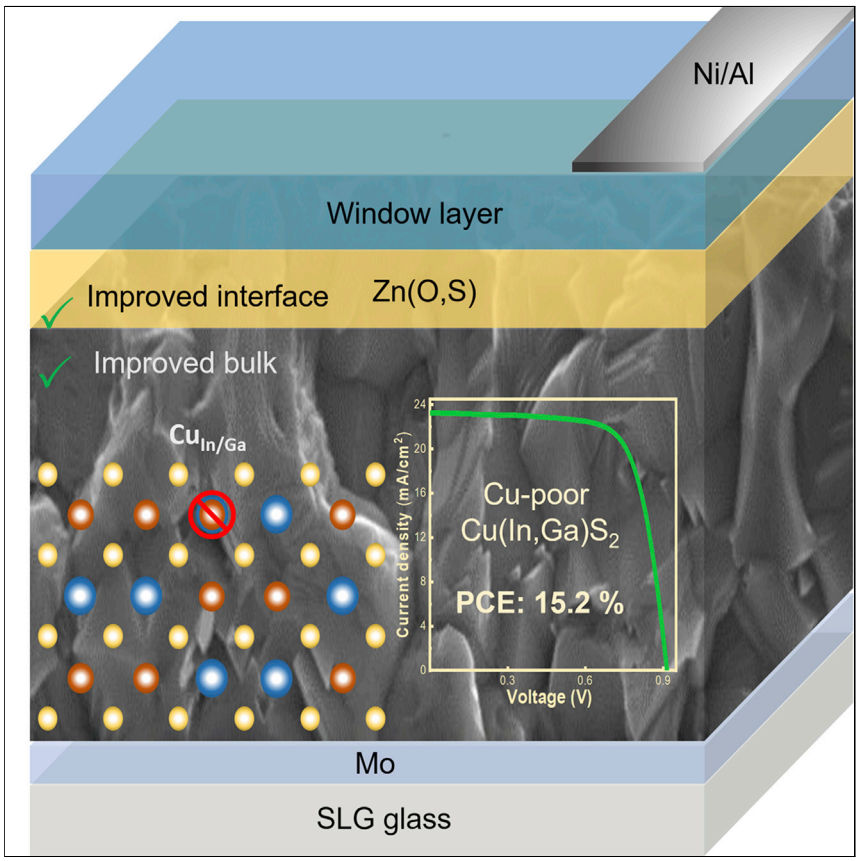

Despite favorable optical properties and band-gap tunability, $Cu(In,Ga)S_2$ solar cell performance is often limited due to bulk and interface recombination losses. We show that Cu-deficient absorbers have lower bulk recombination, owing to the suppression of the detrimental antisite defects. Zn(O,S) buffer layer further lowers the interface recombination due to appropriate band alignment and suppression of defects at the interface. This leads to a high-quality absorber with lower interface losses, resulting in a high power conversion efficiency of over 15%.

Sudhanshu Shukla, Mohit Sood, Damilola Adeleye, ..., Geoffroy Hautier, Rachel Oliver, Susanne Siebentritt

sudhanshu.shukla@uni.lu (S.S.)
susanne.siebentritt@uni.lu (S.S.)

Highlights

Cu deficiency suppresses the bulk recombination losses

Theoretical understanding of bulk defects and its relation to antisite defects

Effective interface passivation using Zn(O,S) buffer layer

High power conversion efficiency from non-toxic H_2S-free and Cd-free process

Shukla et al., Joule 5, 1–16
July 21, 2021
https://doi.org/10.1016/j.joule.2021.05.004

Please cite this article in press as: Shukla et al., Over 15% efficient wide-band-gap Cu(In,Ga)S_2 solar cell: Suppressing bulk and interface recombination through composition engineering, Joule (2021), https://doi.org/10.1016/j.joule.2021.05.004

Joule

CellPress

Article

Over 15% efficient wide-band-gap Cu(In,Ga)S_2 solar cell: Suppressing bulk and interface recombination through composition engineering

Sudhanshu Shukla,[1,5,6,*] Mohit Sood,[1,5] Damilola Adeleye,[1] Sean Peedle,[2] Gunnar Kusch,[2] Diana Dahliah,[3] Michele Melchiorre,[1] Gian-Marco Rignanese,[3] Geoffroy Hautier,[3,4] Rachel Oliver,[2] and Susanne Siebentritt[1,*]

SUMMARY

The progress of Cu(In,Ga)S_2 remains significantly limited mainly due to photovoltage (V_{oc}) losses in the bulk and at the interfaces. Here, via a combination of photoluminescence, cathodoluminescence, electrical measurements, and *ab initio* modeling, we address the bulk and interface losses to improve ~1.6-eV-band-gap (E_g) Cu(In,Ga)S_2. The optoelectronic quality of the absorber improves upon reducing the [Cu]/[Ga+In] (CGI) ratio, as manifested by the suppression of deep defects, higher quasi-Fermi level splitting (QFLS), improved charge-carrier lifetime, and higher V_{oc}. We identify antisite Cu_{In}/Cu_{Ga} as a major performance-limiting deep defect by comparing the formation energies of various intrinsic defects. Interface recombination is suppressed using a Zn(O,S) buffer layer in Cu-poor devices, which leads to the activation energy of recombination equal to the E_g. We demonstrate an efficiency of 15.2% with V_{oc} of 902 mV from a H_2S-free, Cd-free, and KCN-free process.

INTRODUCTION

The efficiency of state-of-the-art photovoltaic technologies is improving every year and coming close to its theoretical limits. For further improvements, new concepts will be needed, among which, tandem solar cells are considered a viable way forward.[1–3] The main criteria for the top cell are suitable band gap, efficiency, and stability.[4] Therefore, sulfide chalcopyrite Cu(In,Ga)S_2, due to its variable band gap between 1.5 and 2.4 eV, is receiving considerable interest as the absorber in the top cell of a tandem device.[5–9]

Cu(In,Ga)S_2 adopts the chalcopyrite structure similar to high-efficiency Cu(In,Ga)Se_2. Despite the high photoconversion efficiency (PCE) of 23.35% achieved using Cu(In,Ga)(S,Se)$_2$,[10,11] the certified record PCE of pure sulfide Cu(In,Ga)S_2 solar cells remained limited to 15.5% thus far.[6] Hence, determining the losses and their underlying origin is of paramount importance to improve the understanding and, consequently, the performance of pure sulfide Cu(In,Ga)S_2 chalcopyrite. A good solar absorber material requires an efficient generation of photocarriers followed by a sustained build-up of charge-carrier density. The latter is directly correlated to quasi-Fermi level splitting (QFLS) and charge-carrier lifetime (τ), often used to analyze the absorber quality. Non-radiative recombination losses reduce the maximum achievable QFLS and lifetime, increasing photovoltage (V_{oc}) deficit. The PCE for Cu(In,Ga)S_2 has remained limited for a long time, mainly due to a large V_{oc} deficit (described as $V_{oc}^{SQ} - V_{oc}$, where V_{oc}^{SQ} stands for Shockley-Queisser V_{oc})[12] of

Context & scale

Cu(In,Ga)S_2 is a high-potential material for its usage in tandem solar cells; however, its power conversion efficiency has remained limited so far. High bulk recombination losses and interface losses both account for the performance limitation. In this work, we adopt a holistic approach to address both bulk and interface recombination losses. We show that bulk recombination losses can be substantially suppressed by controlling the Cu deficiency in the material. From theoretical calculations, we argue that Cu deficiency reduces the antisite defects that are probably the most detrimental defects. Additionally, we effectively passivate the interface through the usage of Zn(O,S) buffer layer, thereby minimizing the losses at the interface. This leads to a solar cell device performance of over 15% from 1.6-eV-band-gap Cu(In,Ga)S_2 from a completely non-toxic process. The path to further performance improvement is discussed to increase the viability of Cu(In,Ga)S_2 toward tandem application.

Please cite this article in press as: Shukla et al., Over 15% efficient wide-band-gap Cu(In,Ga)S_2 solar cell: Suppressing bulk and interface recombination through composition engineering, Joule (2021), https://doi.org/10.1016/j.joule.2021.05.004

more than 300 mV. The latter corresponds to an open-circuit voltage of only 75% of the S-Q limit for V_{oc}, even for the best cell.[6,13–16] Moreover, rather low QFLS and short charge-carrier lifetimes (~hundreds of ps) are typically observed for Cu(In,Ga)S_2.[7,14] This implies significant non-radiative recombination in Cu(In,Ga)S_2. The origin of non-radiative recombination lies in both bulk and interface (front- and back-contact) defects.[17] Concerning the bulk, the low QLFS (and photoluminescence quantum yield [PLQY]) is caused by non-radiative recombination through deep defect states. In this regard, the role of intrinsic point defects in $CuInS_2$ has been highlighted by theoretical studies and photoluminescence analysis, although, much remains unexplored for Cu(In,Ga)S_2.[18–21] The formation of defects and secondary phases depends on the absorber composition.[22] Cu(In,Ga)S_2, or $CuInS_2$, grown under Cu-excess conditions (referred to as Cu-rich) has been extensively explored, owing to the better grain growth and superior optoelectronic properties. Lomuscio et al. showed that (1) the QFLS remains substantially lower than the V_{oc}^{SQ} for both Cu-rich and Cu-poor $CuInS_2$, (2) a higher QFLS value is observed for Cu-rich than Cu-poor $CuInS_2$ and is limited by the deep defects. Additionally, an increase in the QFLS was observed upon an increase in the growth temperature that is consistent with the reduction in the deep defect PL emission intensity. However, it did not translate into an increase in the device V_{oc} due to interface losses.[5] Recently, we found that the improvement in QFLS for Cu-rich absorbers was mainly due to higher doping (D.A. et al., unpublished data). Hiroi et al. demonstrated a record efficiency of 15.5% with an improved Voc of 920 mV, exploiting Cu-poor Cu(In,Ga)S_2 using an optimized ZnMgO buffer layer.[6] The same group later demonstrated a further enhancement in V_{oc} due to rapid thermal annealing (RTA) process, while underscoring the importance of good morphology and Ga back-grading.[14] Kim et al. compared the performance of low-band-gap Cu-poor (1.52 eV) and Cu-rich (1.51-eV) Cu(In,Ga)S_2 absorbers. They observed higher Voc for Cu-poor over Cu-rich Cu(In,Ga)S_2, which was attributed to lower bulk defects and reduced interface recombination in the former.[7] All approaches to increase efficiency relied on toxic H_2S, Cd- and/or KCN-based process. Moreover, the physical insights are still missing. Based on the above-discussed results, we see that non-radiative recombination through deep defects is a major limitation toward performance improvement and requires immediate attention. The physical and chemical understanding of these limiting defects and their relationship with composition need to be understood to improve Cu(In,Ga)S_2.

Apart from bulk-related losses, Cu(In,Ga)S_2 devices suffer from interface recombination, which further limits the Voc. Factors for front surface recombination losses include (1) high defect density at the surface and/or the defects formed during the KCN etching of the $Cu_{2-x}S$ secondary phase for Cu-rich absorbers, which was recently shown to be the case for Cu-rich $CuInSe_2$;[23] and (2) mismatch of the electronic band alignment at the absorber/buffer interface leading to reduced effective interface band gap.[24,25] The extent to which the aforementioned issues can be suppressed depends critically on the choice of the buffer layer. The typically used combination of Cu(In,Ga)S_2/CdS junction forms an energetically non-ideal interface and consequently limits the output Voc.[26–28] A higher energetic position of the Cu(In,Ga)S_2 conduction band minimum to that of CdS (negative band-offset ΔE_c) causes cliff-like electronic-band alignment leading to a reduced recombination barrier at the absorber/buffer interface.[13,25,29,30] Moreover, alloying $CuInS_2$ with Ga leads to a further upshift of the conduction band edge. Therefore, a suitable band alignment with the buffer layer requires further alteration for wide-band-gap Cu(In,Ga)S_2.[31–33] For Cu(In,Ga)S_2/CdS solar cells, the thermal activation energy of the main recombination path deduced from temperature-dependent V_{oc}

[1]Laboratory for Photovoltaics, Department of Physics and Materials Science Research Unit, University of Luxembourg, 44 Rue du Brill, 4422 Belvaux, Luxembourg

[2]Department of Materials Science and Metallurgy, University of Cambridge, Cambridge, UK

[3]Institute of Condensed Matter and Nanosciences, Université catholique de Louvain, Chemin des Étoiles 8, 1348 Louvain-la-Neuve, Belgium

[4]Thayer School of Engineering, Dartmouth College, Hanover, NH 03755, USA

[5]These authors contributed equally

[6]Lead contact

*Correspondence:
sudhanshu.shukla@uni.lu (S.S.),
susanne.siebentritt@uni.lu (S.S.)

https://doi.org/10.1016/j.joule.2021.05.004

Please cite this article in press as: Shukla et al., Over 15% efficient wide-band-gap Cu(In,Ga)S_2 solar cell: Suppressing bulk and interface recombination through composition engineering, Joule (2021), https://doi.org/10.1016/j.joule.2021.05.004

(E_A) were always found to be lower than the band-gap energy, except for the study on Cu-poor Cu(In,Ga)S_2 by Kim et al.[7,34–39] In an attempt to improve the interface configuration from cliff to spike type (positive band-offset ΔE_c), buffer layers with conduction band edge higher than that of Cu(In,Ga)S_2, such as Zn(O,S) and ZnMgO have been explored.[6,14,29,40] Moreover, the higher band gap of these buffer layers allows higher light absorption. Despite a spike-like configuration with Zn(O,S), the activation energy E_A was still found to be lower than the band gap for Cu-rich Cu(In,Ga)S_2.[29] These results suggest that Cu-rich Cu(In,Ga)S_2 is highly prone to interface recombination. Furthermore, Cu-poor Cu(In,Ga)S_2 provides a promising avenue to address the issue of interface recombination losses. Finally, back-contact recombination accounts for additional losses that need to be suppressed to realize high V_{oc}. In the related selenide chalcopyrite solar cells, this issue is tackled by a Ga gradient, providing a higher conduction band edge and thus fewer minority carriers near the back contact.[41–43] Therefore, the major challenge is to reduce non-radiative recombination in the bulk and to suppress front and back surface recombination to realize better performance.

We address these challenges by; (1) Cu-composition engineering of Cu(In,Ga)S_2, especially exploring Cu-poor regime, (2) buffer layer engineering, and (3) Ga grading to prevent backside recombination. In this work, we exploit the above-mentioned factors by adopting a multistage co-evaporation process to prepare ~1.6-eV-band-gap Cu(In,Ga)S_2. The multistage deposition process allows better control of morphology and helps in attaining a Ga profile.[44,45] We methodically investigate the effect of varying [Cu]/[Ga+In] (CGI) ratios on the optoelectronic quality of the bulk. As an indicator of the bulk optoelectronic quality and a representative of the maximum achievable V_{oc}, we determine QFLS from room-temperature photoluminescence (PL) spectroscopy and compare the absorbers with varying CGI.[46,47] Non-radiative recombination losses in the bulk reduce the QFLS from the Shockley-Queisser (SQ) limit and recombination losses at the interface lead to V_{oc} lower than the QFLS, as the splitting is lower at the interface due to excess carrier loss. Hence, a V_{oc} deficit with respect to QFLS indicates recombination losses at the interface.[48,49] We show that QFLS increases as the Cu(In,Ga)S_2 films become more Cu-poor, still keeping the CGI ratio above 0.9, along with a reduction in the deep defect PL intensity. This is accompanied by an increase in the carrier lifetime from transient photoluminescence (TRPL) analysis. We did not study the films with CGI < 0.9 in the present manuscript. We further assess the impact of CdS and Zn(O,S) buffer layers on device characteristics of Cu-poor and Cu-rich Cu(In,Ga)S_2 solar cells. We demonstrate that passivation effect in Cu-poor Cu(In,Ga)S_2/Zn(O,S) devices leads to an increase in the V_{oc} very close to QFLS, indicating the suppression of interface recombination. This effect is also confirmed by the activation energy of the saturation current deduced from temperature-dependent V_{oc} extrapolating to the band gap of the absorber. Remarkably, this passivation effect of Zn(O,S)/ Cu(In,Ga)S_2 device is only effective for Cu-poor composition. As a result, Zn(O,S) buffer layer Cu-poor devices demonstrate an efficiency above 15% with a low V_{oc} deficit of 388 mV.

RESULTS AND DISCUSSION

This study is conducted on Cu(In,Ga)S_2 thin films with CGI ratio between 0.93 and 1.29 having similar [Ga]/[Ga+In] (GGI) of 0.12–0.18. The films are grown by multistage or single-stage processes, see Figure 1 (refer to the experimental procedures and Figure S1 for details). We first investigate the structural properties of the film and subsequently investigate the optoelectronic properties of the film in terms of QFLS and the nature of non-radiative recombination losses, with a particular focus on deep

Please cite this article in press as: Shukla et al., Over 15% efficient wide-band-gap Cu(In,Ga)S_2 solar cell: Suppressing bulk and interface recombination through composition engineering, Joule (2021), https://doi.org/10.1016/j.joule.2021.05.004

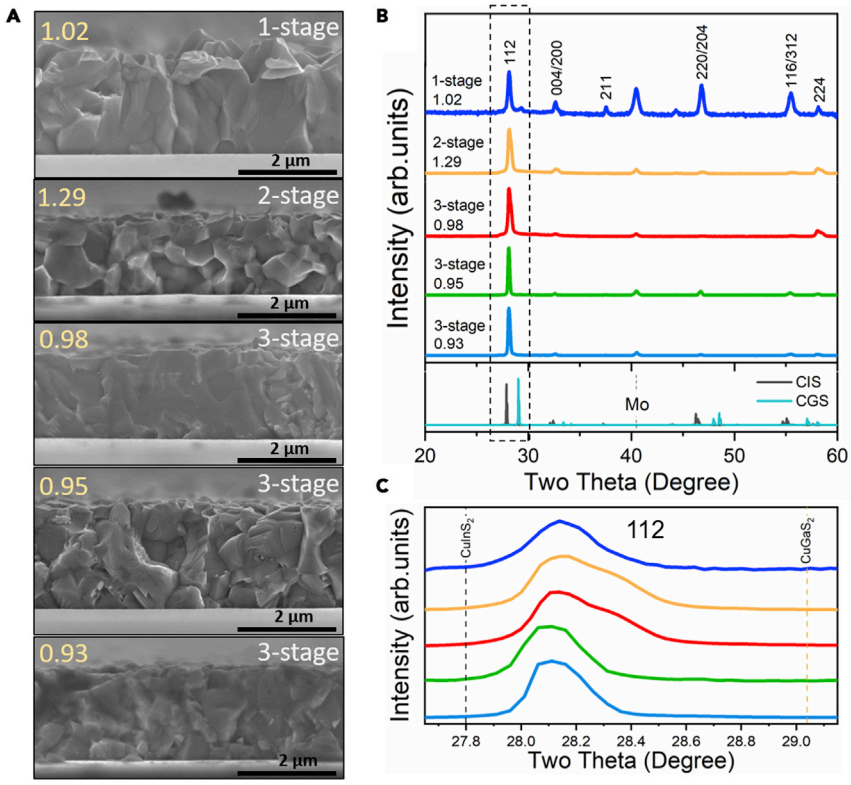

Figure 1. Structural characterization of Cu(In,Ga)S_2 thin films with varying CGI ratios

(A) Cross-section SEM micrograph of 1-stage, 2-stage, and 3-stage processed absorbers with varying CGI ratios (see also Figure S2).

(B and C) (B) Corresponding XRD diffractograms of the Cu(In,Ga)S_2 thin films on Mo substrate and (C) dominant (112) reflection indicating the peak broadening (see also Figure S3). Reference scans for $CuInS_2$ (CIS) and $CuGaS_2$ (CGS) Taken from ICSD 186714 and ICSD 28736, respectively.[50]

defects. We correlate the absorber composition to the performance of devices made with CdS and Zn(O,S) buffer layers. We explore the differences in bulk and interface of Cu-poor and Cu-rich composition by absolute calibrated and time-resolved photoluminescence, capacitance measurements, and temperature-dependent V_{oc} measurements. Finally, we demonstrate high-quality bulk and interface-passivated Cu-poor Cu(In,Ga)S_2 solar cells.

Structural characterization and morphology

Figure 1A shows the microstructural features of the 1-stage, 2-stage, and 3-stage processed films with varying CGI ratios, as seen by cross-sectional scanning electron (SE) imaging (see top-view SEM image in Figure S2). The 1-stage processed near stoichiometric absorber Cu(In,Ga)S_2 (1.02) exhibits large columnar grains and rough surface, consistent with the previous observation from Ga-free $CuInS_2$.[5] Grain boundaries in Cu-rich Cu(In,Ga)S_2 provide shunting paths for the carriers and are deleterious to the device performance.[5,51] The 2-stage Cu-rich Cu(In,Ga)S_2 (1.29) sample's SE micrograph is acquired after etching the CuS_x secondary phase, which exists in Cu-rich absorbers.[52] During the second growth stage beyond the stoichiometric point, CuS_x forms at the surface and assists in grain growth and sulfur incorporation.[53] It is evident from the SE images that 2-stage Cu-rich Cu(In,Ga)S_2 exhibits compact grains with smooth surface morphology. A different Cu-poor composition is achieved by adjusting the duration of the final (third) stage of the growth process. For 3-stage Cu(In,Ga)S_2 films, the grain size appears to be reduced as the CGI is

Please cite this article in press as: Shukla et al., Over 15% efficient wide-band-gap Cu(In,Ga)S_2 solar cell: Suppressing bulk and interface recombination through composition engineering, Joule (2021), https://doi.org/10.1016/j.joule.2021.05.004

diminished. Notably, SE images also reveal smaller grains near the Mo interface. Yet, the morphology seems more favorable with larger grains than in Cu-poor 1-stage films.[5] To probe the phase and orientation of the films, θ-2θ X-ray diffractograms (XRD) of the Cu(In,Ga)S_2 films were recorded, as shown in Figure 1B. All the diffraction peaks could be indexed to a chalcopyrite structure and to the Mo back contact ($CuInS_2$: ICSD 186714 and $CuGaS_2$: ICSD 28736). Compared with the reference powder diffraction pattern of $CuInS_2$, diffraction peaks of the samples shift to higher angles depending on the GGI ratio. Substitution of In with smaller Ga leads to lattice contraction and shrinkage of the unit cell volume resulting in the shift of diffraction peaks to higher angles. GGI ratios for all the films are in the range 0.12–0.18; hence, the peak shift is relatively similar for all the films. It is known that the formation kinetics of $CuGaS_2$ and $CuInS_2$ are different, and the growth front of the absorber is located at the surface.[53,54] The consequence of this is the in-depth Ga-grading profile, which depends on the growth temperature, growth profile (stages), and deposition rates. Ga grading is manifested by peak broadening in the XRD pattern. Examining the dominant (112) reflection peak reveals asymmetric peak broadening. From Figure 1C, the 1-stage Cu(In,Ga)S_2 (1.02) film shows a symmetric (112) diffraction peak, suggesting negligible Ga grading for this particular film. On the other hand, 2-stage and 3-stage films show a shoulder extending toward higher angles, corroborating the Ga-grading profile in the absorbers (see secondary ion mass spectroscopy [SIMS] elemental profile in Figure S3).

Photoluminescence and cathodoluminescence—band gap (E_g), QFLS, and defect analysis

Before analyzing the defects and optoelectronic quality, we determine the band gap of the absorbers from photoluminescence spectroscopy.

Figure 2A shows normalized and baseline shifted room-temperature PL spectra. The PL peak corresponds to band-band transition for the samples with varying CGI ratios. Thus, we set the energy of the PL maximum equal to the band gap. In the case of Ga grading, this is expected to represent the minimum band gap in the film.[55] All the samples showed a band gap value in the range 1.57–1.61 eV observed from the peak maxima (band gap from quantum efficiency is shown in Figure S4). Specific values of the band gap determined from PL are listed in Table 1. We deduced QFLS values from absolute calibrated PL at photon fluxes equivalent to 1 Sun (Table 1), similar to the method described in the study conducted by Babbe et al.[56] We observed a decrease in the QFLS deficit as the CGI ratio was reduced. As an exception, a lower QFLS deficit was observed for the 1-stage absorber on comparing the near stoichiometric 1-stage and 3-stage Cu(InGa)S_2. The presence of a high density of defects, deep traps, and associated Shockley-Read-Hall (SRH) non-radiative recombination is a major challenge for these sulfide absorbers that must be addressed to reduce QFLS deficit (V_{oc}^{SQ} – QFLS). Therefore, to interpret the QFLS losses, we acquired PL spectra at 20 K to study defects. From Figure 2B, it can be observed that a characteristic feature of the Cu-rich absorber is the appearance of two predominant peaks close to the band edge followed by broad deep defect emission at about ~1.3 eV (referred to as D1) and 1.1 eV (referred to as D2). (Gaussian peak fits of the PL peaks for all the films are shown in Figure S5.) In addition, for the near stoichiometric Cu-poor Cu(In,Ga)S_2, a single predominant peak close to the band edge is observed, followed by the D1 and D2 emissions. Interestingly for 3-stage Cu(In,Ga)S_2, we noticed a drastic suppression in the D1 and D2 emission and an increase in the QFLS as CGI was reduced, indicating higher radiative recombination (Figure 2C). The suppression of these deep defect states reduces SRH-type non-radiative recombination. Indeed, the trend in QFLS deficit is in agreement with the low-

Please cite this article in press as: Shukla et al., Over 15% efficient wide-band-gap Cu(In,Ga)S_2 solar cell: Suppressing bulk and interface recombination through composition engineering, Joule (2021), https://doi.org/10.1016/j.joule.2021.05.004

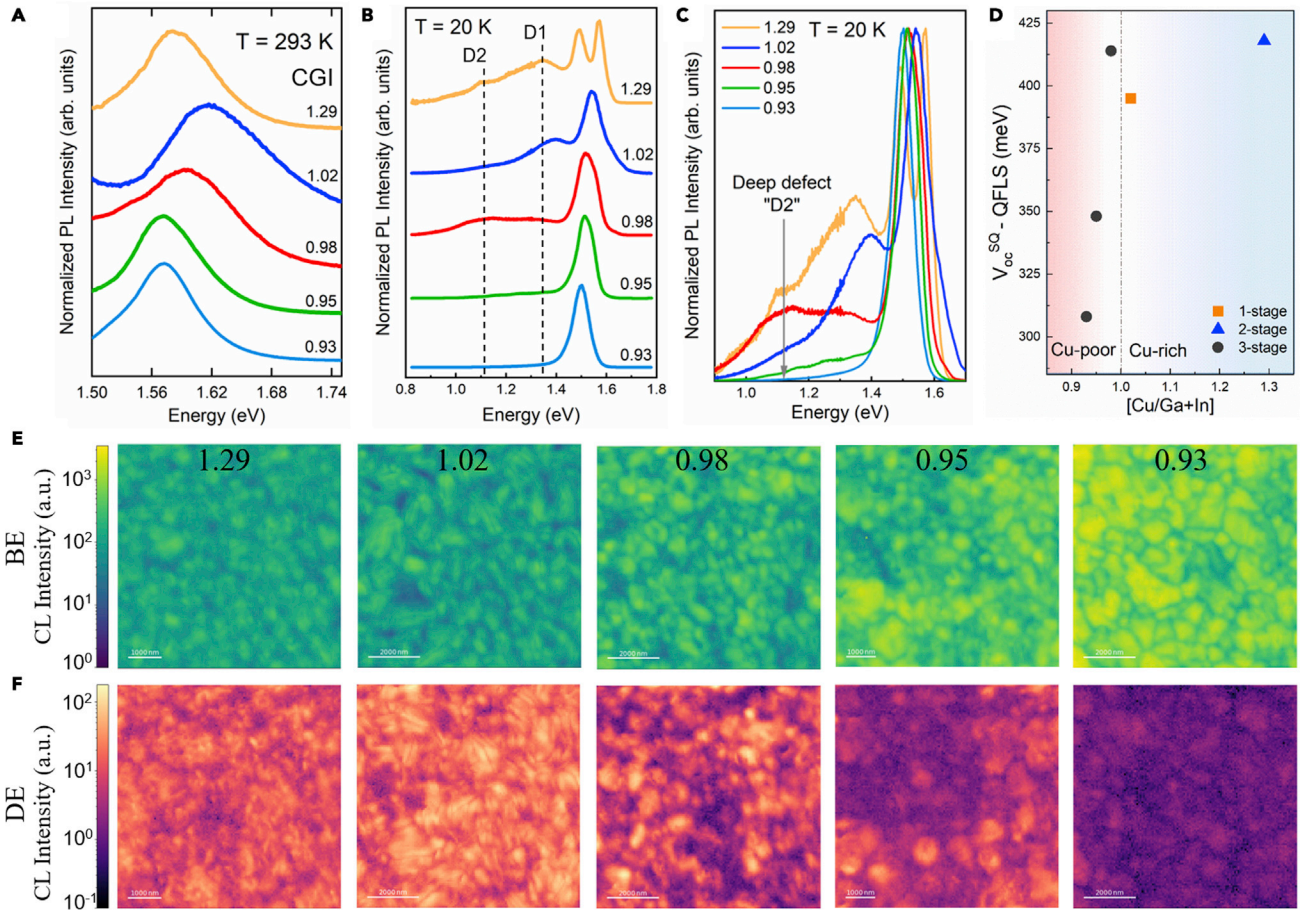

Figure 2. QFLS deficit and defect analysis from photoluminescence and cathodoluminescence measurements

(A–D) Normalized and baseline shifted PL spectra at (A) room temperature and (B) low temperature (20 K), (C) PL spectra at 20 K normalized to their respective band-edge peak, and (D) QFLS deficit of the Cu(In,Ga)S_2 films with varying CGI ratios (see also Figure S4).

(E and F) Room-temperature cathodoluminescence mapping of Cu(In,Ga)S_2 films with varying CGI ratios (E) CL intensity map of the band-related emission (BE) at 1.6 eV and (F) defect emission (DE) at 1.3 eV (D1) (see also Figure S5).

temperature PL interpretation, as shown in Figure 2D. QFLS deficit value is lower for the absorber with suppressed deep defect PL emission as the CGI is reduced. The QFLS deficit with respect to the band gap of the respective films allows quantitative comparison of the absorber quality. The values are summarized in Table 1. Thus, the upper limit of the QFLS is set by the lowest energy defect level/band, D2 in this case. This becomes more obvious when comparing Cu-poor film (0.98) with Cu-rich film (1.29), which exhibit comparable QFLS values despite their difference in the composition. This is because, while D1 is suppressed for the slightly Cu-poor film, the presence of D2 similar to the Cu-rich film limits the QFLS in the same way. In principle, higher QFLS in the Cu-poor absorbers could be due to higher doping. However, later we show that the doping is considerably lower in Cu-poor films along with longer minority carrier lifetimes, indicating that it is, indeed, the reduction of non-radiative recombination centers that lead to the higher QFLS in Cu-poor films. To investigate the microscopic origin of the recombination process, cathodoluminescence (CL) hyperspectral imaging was performed. The high spatial resolution of the CL allows correlation of microscopic features to luminescence characteristics. CL spectra for these films exhibit two peaks; band-band emission (BE) close to 1.6 eV and defect emission (DE) close to 1.3 eV (D1), consistent with the PL measurements (see Figure S5).

Please cite this article in press as: Shukla et al., Over 15% efficient wide-band-gap Cu(In,Ga)S_2 solar cell: Suppressing bulk and interface recombination through composition engineering, Joule (2021), https://doi.org/10.1016/j.joule.2021.05.004

Table 1. Cu(In,Ga)S_2 with varying CGI ratios with corresponding values of E_g, QFLS, and QFLS deficit derived from room-temperature photoluminescence

CGI[a]	E_g (eV)[b]	QFLS (meV)[c]	V_{oc}^{SQd} – QFLS (meV)
Cu(In,Ga)S_2 (1.29)	1.58	872	418
Cu(In,Ga)S_2 (1.02)	1.61	923	395
Cu(In,Ga)S_2 (0.98)	1.59	885	414
Cu(In,Ga)S_2 (0.95)	1.58	942	348
Cu(In,Ga)S_2 (0.93)	1.57	972	308

[a][Cu]/[Ga+In] [a]Band gap
[b]Quasi-Fermi level splitting
[c]Shockley-Queisser limit of photovoltage; SQ limit of the photovoltage

Figures 2E and 2F shows the color maps of the lateral CL intensity distribution from CL hyperspectral mapping corresponding to BE and DE emission, respectively, for varying CGI ratios. Note that, the CL spectra were acquired under identical measurement conditions for all the samples to facilitate comparison of the emission intensities. It is clear that as the Cu deficiency is increased, BE intensity is increased in agreement with the PL spectra with a simultaneous decrease in the DE intensity (defect D1). There is a decrease in non-radiative recombination associated with the reduction in the defect concentration. Thus, from PL and CL, we find a reduction in both D1 and D2 defects. The appearance of the DE signal from the grain interior indicates defect distribution in the bulk as well. Intensity contrast in the CL map reveals darker grain boundaries (GB), implying significant losses due to non-radiative recombination at GBs. The contrast between different grains could arise due to topography. Surface topography can affect the generation rate of electron-hole pairs in the sample rather strongly. However, previous studies of related materials have shown that GB may act as non-radiative recombination centers.[57] Further investigations providing a detailed analysis of the influence of GB are ongoing. To summarize, the defects and non-radiative recombination are strongly suppressed in Cu-deficient Cu(In,Ga)S_2 films, leading to higher QFLS.

Defect model

The question arises as to what the chemistry of the defect level D2 is that is reduced by lower Cu content and limits the QFLS in these absorbers. The study of intrinsic point defects, of the nature of dominant point defects (i.e., shallow or deep), and how their concentration varies with respect to growth conditions is possible through density functional theory (DFT). The accuracy of predicting the position of the thermodynamic transition levels in the band gap and their respective formation energies are highly dependent on the details of the theoretical methods, notably the choice of the exchange-correlation functional. We adopt the hybrid Heyd-Scuseria-Ernzerhof (HSE) functional, which has become the standard for defect computations as it provides a more accurate band gap than semi-local functionals. The calculation results are shown in Figure 3. Intrinsic vacancy and antisite defects are the most prominent electronic defects in chalcopyrite.[58] To understand the defect in Cu(In,Ga)S_2, we performed defect calculations for $CuInS_2$ and $CuGaS_2$. From Figure 3, three deep defects in $CuInS_2$ and $CuGaS_2$ can be identified: the vacancies of the group III element—which rather have high formation energies (>3 eV) in both cases for all compositions considered—and the two antisite defects (Cu_{III} and III_{Cu}).

The first observation is that the formation energies of the Cu vacancy and Cu_{In}/Cu_{Ga} are similar in both compounds. In contrast, the formation energies of the other intrinsic defects (i.e., Ga_{Cu}, V_{Ga}, and V_S) are higher in $CuGaS_2$ than in $CuInS_2$. The deep antisite of Cu_{III} is the dominant defect in the regions A, F, and G, which represents the Cu-rich and

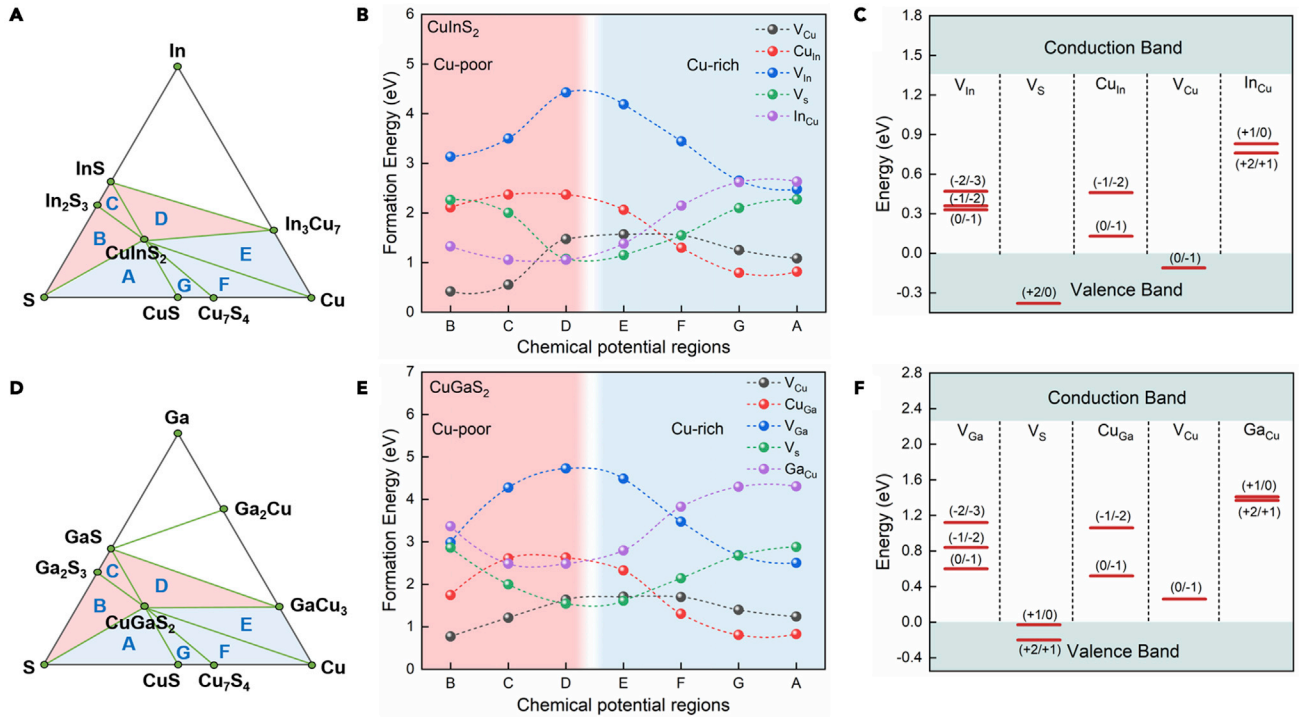

Figure 3. Theoretical analysis of the defect formation energies and their energetic position in $CuInS_2$ and $CuGaS_2$

(A and D) (A) $CuInS_2$ and (D) $CuGaS_2$ phase diagrams, and the calculated stable chemical-potential regions in specific facets labeled from A to G (left).

(B and E) These show the neutral intrinsic defect formation energies corresponding to various chemical potential at the regions A–G as shown in the phase diagram.

(C and F) These show the calculated defect transition energy levels of intrinsic point defects in the band gap for $CuInS_2$ and $CuGaS_2$, respectively (see also Figure S6).

S-rich domain, where it has the lowest formation energy. The defect transition levels for the different point defects are depicted in Figures 3C and 3F (see also Figure S6). Cu_{In} has a (second) charge transition level at 0.46 eV from the valence band maximum (VBM), in agreement with previous reports.[18,59] This energy level could agree with the experimental transition energy observed for the D2 defect. Cu_{Ga} has deeper levels. The energetic location of the Cu_{In} antisite defect along with the low formation energy in the high Cu-composition range (F-G-A) would result in high charge-carrier recombination and consequently short carrier lifetimes. On the other hand, the Cu_{In}/Cu_{Ga} antisite has a high formation energy in the Cu-poor compositional range (B-C-D), making it less prominent. In contrast, the In_{Cu}/Ga_{Cu} antisite has the lowest formation energies in the B, C, and D compositional ranges; i.e., it could be present under low-Cu compositions. From these results, the deep defects D1 and D2, which decrease under Cu-poor conditions, could be related to the Cu_{III} antisite, which is expected to have a lower concentration in Cu-poor conditions.

Device characteristics of Cu-poor and Cu-rich Cu(In,Ga)S_2: V_{oc} deficit and interface losses

To compare the difference between Cu-poor and Cu-rich Cu(In,Ga)S_2 in terms of device performance, we chose absorbers with similar QFLS deficit, i.e., with the same bulk quality. QFLS of slightly Cu-poor (885 meV) Cu(In,Ga)S_2 was marginally higher than that of the Cu-rich Cu(In,Ga)S_2 (872 meV). Comparing the QFLS deficit with respect to the V_{oc}^{SQ} showed the same value within error (418 meV for Cu-poor and 414 meV for Cu-rich Cu(In,Ga)S_2), indicating that the samples were very similar in terms of their optoelectronic quality. Specific features in the dark and illuminated

Please cite this article in press as: Shukla et al., Over 15% efficient wide-band-gap Cu(In,Ga)S_2 solar cell: Suppressing bulk and interface recombination through composition engineering, Joule (2021), https://doi.org/10.1016/j.joule.2021.05.004

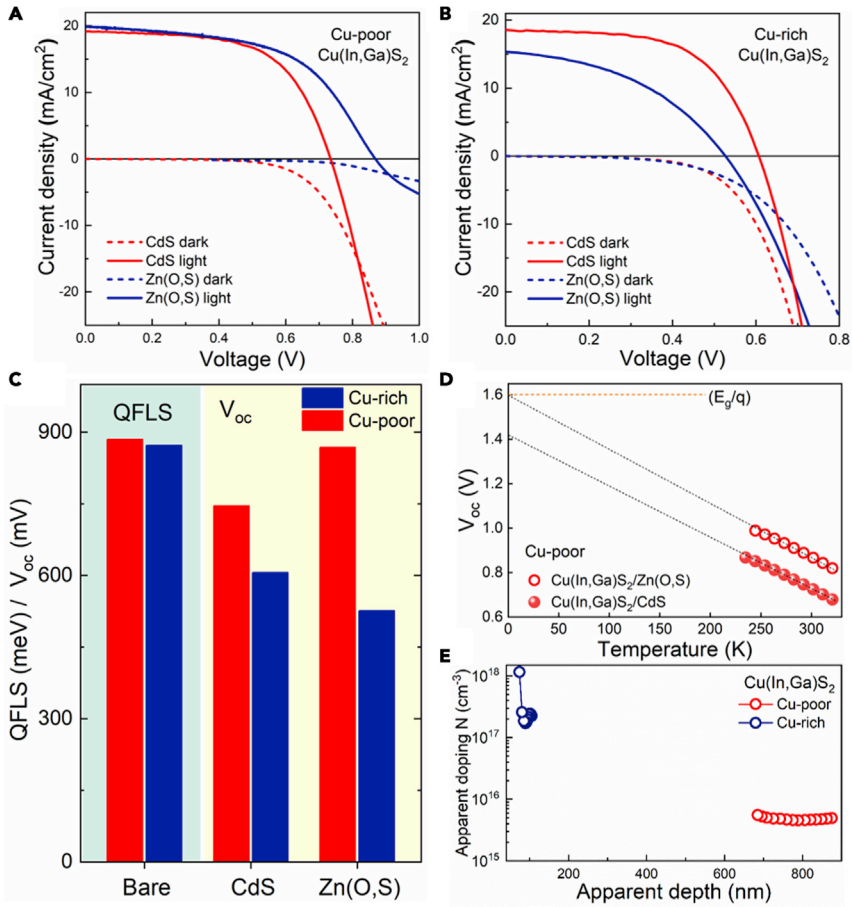

Figure 4. Optoelectronic comparison between Cu-poor and Cu-rich Cu(In,Ga)S_2 solar cells

(A–C) Dark and illuminated (without light soaking) current-voltage (J-V) characteristics of the (A) Cu-poor and (B) Cu-rich solar cells with different buffer layer under AM 1.5 illumination (see also Figure S7), and (C) comparison of QFLS and photovoltage of Cu(In,Ga)S_2 devices with different buffer layers (see also Figure S8)

(D and E) (D) V_{oc} versus temperature plot for Cu-poor Cu(In,Ga)S_2 with CdS and Zn(O,S) solar cell and (E) carrier concentration deduced from C-V measurements performed on Cu-poor and Cu-rich devices with a CdS buffer layer.

J-V curves are related to various types of defects and/or barriers for current flow. Analysis of J-V curves in Figures 4A and 4B show different features for CdS and Zn(O,S)-based solar cells. We noticed crossover and rollover effects in the J-V curves.

Crossover effects are generally observed in chalcopyrite devices. They are related to a photo-dependent barrier for electron flow due to several reasons—band offsets at the absorber-buffer and buffer-window interface, defective chalcopyrite layer near the absorber surface, defects at the buffer/window interface.[43,60] Figure 4A shows crossover in the J-V curves for Cu-poor Cu(In,Ga)S_2 solar cells with CdS and Zn(O,S) buffer layers. Also, a similar crossover is observed in the J-V curve for Cu-rich Cu(In,Ga)S_2 solar cells with Zn(O,S) buffer layer, as shown in Figure 4B. The higher conduction band minimum of Zn(O,S) favors the formation of the desired spike-like conduction band alignment, which helps in reducing interfacial recombination.[29] The fact that crossover is more pronounced in the case of Zn(O,S) buffer layer, for both Cu-poor and Cu-rich Cu(In,Ga)S_2 solar cells, indicates that the behavior is related to the spike at the absorber/buffer and cliff at the buffer/window layer. An

Please cite this article in press as: Shukla et al., Over 15% efficient wide-band-gap Cu(In,Ga)S_2 solar cell: Suppressing bulk and interface recombination through composition engineering, Joule (2021), https://doi.org/10.1016/j.joule.2021.05.004

Table 2. Solar parameters of the devices presented in Figures 4A and 4B

Cu(In,Ga)S_2 device	V_{oc}[a] (mV)	J_{sc}[b] (mA/cm^2)	FF[c] (%)	PCE[d] (%)	QFLS[e] - V_{oc} (mV)
Cu-poor/ CdS	734	19.1	60.7	8.6	151
Cu-poor/ Zn(O,S)	868	19.9	54.9	9.5	17
Cu-rich/ CdS	607	18.5	59.7	6.7	265
Cu-rich /Zn(O,S)	527	15.4	42.6	3.5	345

[a]Photovoltage
[b]Photocurrent
[c]Fill-factor
[d]Photo-conversion efficiency
[e]Quasi-Fermi level splitting

additional rollover effect is observed for the Cu-poor solar cell with Zn(O,S) buffer layer. This reduction of the forward current in the dark and under illumination indicates potential barrier(s) for the majority carrier flow (injection barrier), which could be due to window/buffer band alignment.[61–63] (refer to the simulations in Figure S7) The above-discussed interface issues influence the recombination and impact the output V_{oc}. To understand the V_{oc} losses, we compared the V_{oc} of the solar cells fabricated with CdS and Zn(O,S) buffer layers, as shown in Figure 4C (see also in Figure S8).

Our first observation is that the V_{oc} values for the devices with CdS buffer remain considerably lower than the QFLS values regardless of the composition. This observation indicates severe losses due to recombination near or at the interface(M.S. et al., unpublished data).[48,49] Second, the V_{oc} of the Cu-poor Cu(In,Ga)S_2 devices with Zn(O,S) buffer shows marked improvement with a value very close to the QFLS. As evident from Table 2, the Zn(O,S) buffered solar cell achieves V_{oc} close to the QFLS value (measured on the bare absorber) with an increase of 122 mV compared with CdS buffer-based solar cells (highlighted in Table 2), indicating V_{oc} gain from reduced interface recombination losses.

To validate our conclusion on interface recombination from J-V analysis and QFLS, we analyzed the temperature dependence of V_{oc} obtained from J-V characteristics. The temperature-dependent V_{oc} helps identify the dominant recombination mechanism such as bulk (SRH) or interface recombination. The temperature-dependent V_{oc} is expressed by the following relation[43,64]

$$V_{oc} = \frac{E_A}{q} - \frac{\xi k_B T}{q} \ln\left(\frac{J_{00}}{J_{sc}}\right) \quad (Equation 1)$$

Where E_A is the activation energy of the rate of the main recombination path, k_B is the Boltzmann constant, ξ is the diode ideality factor, J_{sc} is the photocurrent density, and J_{00} is the prefactor to the saturation current density. The activation energy is found from the V_{oc} intercept at T = 0 K obtained by linear extrapolation of V_{oc} at high temperatures. The ideality factor remained temperature independent in the high-temperature linear range used for extrapolation (240–320 K). Below 240 K, devices show strong rollover effect. From Figure 4D, E_A value for Cu-poor solar cells with CdS buffer layer extrapolates to ~1.42 eV, a value less than the band gap of the absorber (from PL E_g^{PL}: 1.59 eV and external quantum efficiency (EQE) $E_g^{d(EQE)/dE}$: 1.60 eV). Thus, CdS-based devices suffer from interface recombination, consistent with previous observations.[29,36] On the contrary, E_A for the Zn(O,S) buffered device extrapolates to 1.60 eV, a value equal to the band gap, implying these devices are not limited by interface recombination and are dominated by bulk recombination. These results reveal the importance of a suitable buffer and interface band-offset engineering for the passivation of interface recombination. In addition,

Please cite this article in press as: Shukla et al., Over 15% efficient wide-band-gap Cu(In,Ga)S_2 solar cell: Suppressing bulk and interface recombination through composition engineering, Joule (2021), https://doi.org/10.1016/j.joule.2021.05.004

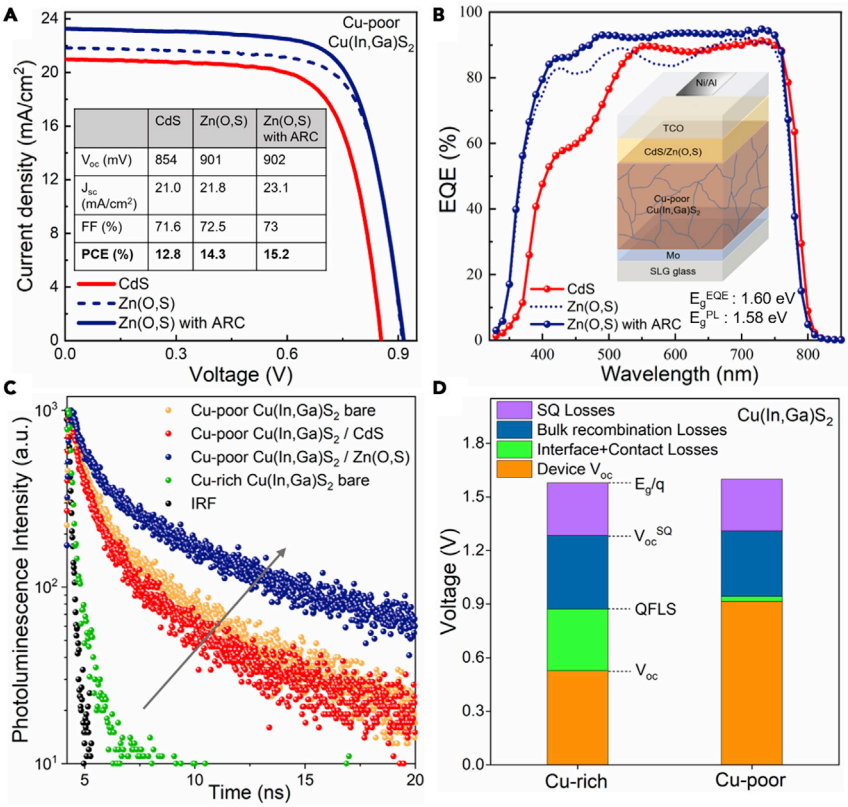

	CdS	Zn(O,S)	Zn(O,S) with ARC
V_{oc} (mV)	854	901	902
J_{sc} (mA/cm^2)	21.0	21.8	23.1
FF (%)	71.6	72.5	73
PCE (%)	**12.8**	**14.3**	**15.2**

Figure 5. High-efficiency solar cell from Cu-poor Cu(In,Ga)S_2

(A–D) (A) J-V characteristics and (B) EQE for 15 mins light-soaked Cu-poor Cu(In,Ga)S_2 with CdS and Zn(O,S) solar cell (see also Figures S9, S10, and S11), (C) PL decay curves for bare Cu-rich (1.29) and Cu-poor (0.93) and films and with buffer layers at room temperature (the arrow indicates improved lifetime for Cu-poor absorber and with Zn(O,S) buffer), (laser excitation wavelength: 640 nm; IRF, instrument response function), and (D) V_{oc} loss analysis for Cu-rich and Cu-poor Cu(In,Ga)S_2 devices with Zn(O,S) buffer layer.

this passivation effect is rather dependent on the composition of the absorber. Notably, interface recombination is found to be a performance-limiting factor for Cu-rich Cu(In,Ga)S_2 devices even with a suitable Zn(O,S) buffer, consistent with the previous report.[29] It is worth highlighting that activation energy close to band-gap value is rarely reported for pure sulfide Cu(In,Ga)S_2 solar cells. Collectively, these results demonstrate that the Zn(O,S) buffer is effective in suppressing the interface recombination in Cu-poor Cu(In,Ga)S_2 mainly due to well-aligned band offsets, whereas Cu-rich Cu(In,Ga)S_2 remain prone to interface recombination, most likely due to a damaged surface, similar to Cu-rich selenide absorbers.[23] Thus, Cu-poor absorbers are promising to achieve higher V_{oc}. We performed capacitance-voltage (C-V) measurements on the devices to analyze the carrier density in the Cu-poor and Cu-rich Cu(In,Ga)S_2, as shown in Figure 4E. The Cu-rich absorber exhibits a high carrier density, while it is significantly lower for Cu-poor absorbers, indicating a high degree of compensation.

High-efficiency solar cells from Cu-poor Cu(In,Ga)S_2

Based on our detailed optoelectronic investigations, we found that Cu-poor Cu(In,Ga)S_2 absorber with CGI of 0.93 exhibit considerably lower QFLS deficit, and therefore a better solar cell performance is expected, suitable for high-

Please cite this article in press as: Shukla et al., Over 15% efficient wide-band-gap Cu(In,Ga)S_2 solar cell: Suppressing bulk and interface recombination through composition engineering, Joule (2021), https://doi.org/10.1016/j.joule.2021.05.004

performing solar cells. Using Cu(In,Ga)S_2 with CGI of 0.93, we prepared devices with CdS and Zn(O,S). Figure 5A shows the J-V characteristics and summarizes the photovoltaics (PV) parameters of the best devices. Highest photoconversion efficiency (PCE) of 12.8% and 15.2% is obtained for CdS and Zn(O,S) solar cells, respectively (statistical distribution of PCE for 12 devices is shown in Figure S9) In both cases, light soaking is required to remove the kink in the J-V curve, consequently improving the fill factor (FF) and overall PCE of the device (See dark current in Figure S10 and light-soaking effect on the device in Figure S11). V_{oc} is significantly higher for the Zn(O,S) buffer device (902 mV), which corresponds to a V_{oc}^{SQ} deficit of 400 mV for a 1.6-eV-band gap. The higher V_{oc} is due to the higher QFLS, i.e., better optoelectronic quality of the absorber, and due to less V_{oc} loss compared with QFLS, i.e., better quality of the interface due to a more suitable conduction band alignment with the Zn(O,S) buffer layer. In addition, the larger band gap of Zn(O,S) buffer layer enables absorption of higher energy photons resulting in a higher short-circuit current density (J_{sc}), consistent with the photocurrent gain shown in the EQE Figure 5B. Applying anti-reflective coating (ARC) leads to improvement in the J_{sc}, as evident from the recovery of reflection losses in the EQE, resulting in an overall PCE of 15.2%. Regarding the stability, both CdS-based and Zn(O,S) devices show similar behavior. However, the stability of these devices are yet to be quantified in the context of different stresses such as environmental conditions and light soaking.

This demonstrates that pure sulfide Cu(In,Ga)S_2 solar cells could function remarkably similar to pure-selenide-based solar cells. The excellent performance is not only due to better optoelectronic quality of the Cu-poor absorbers but also benefits from a Ga-grading profile. (The in-depth composition profile from SIMS are presented in Figure S3.) Our film shows a double-graded Ga profile with higher Ga at the back and the front. A relatively wide and flat region of Ga distribution and modest Ga gradient suppresses recombination at the back contact.[44] The advantage of Ga gradient has been observed previously for RTA Cu(In,Ga)S_2 absorbers.[14] Ga-grading profile could be further optimized for higher performance. Finally, we compare the carrier lifetime of the Cu-poor and Cu-rich Cu(In,Ga)S_2 from room-temperature transient photoluminescence (TRPL). From Figure 5C, a bi-exponential PL decay characteristic is observed for bare Cu-poor and Cu-rich absorbers. Cu-poor Cu(In,Ga)S_2 shows significantly longer lifetimes (τ_{fast}: 500 ps and τ_{slow}: 3.2 ns) than the Cu-rich absorber (τ_{fast}: 176 ps and τ_{slow}: 1.2 ns).

The longer lifetime in Cu-poor Cu(In,Ga)S_2 is attributed to the suppression of SRH-recombination, in agreement with the steady-state low-temperature photoluminescence analysis and higher QFLS. The PL decay lifetime is improved further for the Cu-poor Cu(In,Ga)S_2/ Zn(O,S) stack (τ_{fast}: 605 ps and τ_{slow}: 4.5 ns), corroborating the surface passivation effect of Zn(O,S). From Figure 5D, analysis of V_{oc} losses in Cu-rich and Cu-poor Cu(In,Ga)S_2 devices with Zn(O,S) buffer layer reveals lower bulk recombination and substantial suppression in interface recombination for Cu-poor Cu(In,Ga)S_2. This highlights the importance of Cu stoichiometry and composition in Cu(In,Ga)S_2 for further efficiency enhancement. Figure 6A shows the reported V_{oc} values for Cu-poor and Cu-rich $CuInS_2$ and Cu(In,Ga)S_2 solar cells. For higher-band-gap absorbers, the V_{oc}^{SQ} deficit is better for Cu-poor absorbers. Recently, an efficiency close to 12% was reported for 1.6-eV-band-gap selenide-$CuGaSe_2$-based solar cells with record V_{oc} of 1,003 mV with $Zn_{1-x}Sn_xO_y$ (ZTO) buffer layer.[65] The higher efficiency for the similar 1.6-eV-band-gap absorber reported in this study (Figure 6B) demonstrates that sulfide absorbers could be an excellent choice for the top cell in tandem solar cells.

Please cite this article in press as: Shukla et al., Over 15% efficient wide-band-gap Cu(In,Ga)S_2 solar cell: Suppressing bulk and interface recombination through composition engineering, Joule (2021), https://doi.org/10.1016/j.joule.2021.05.004

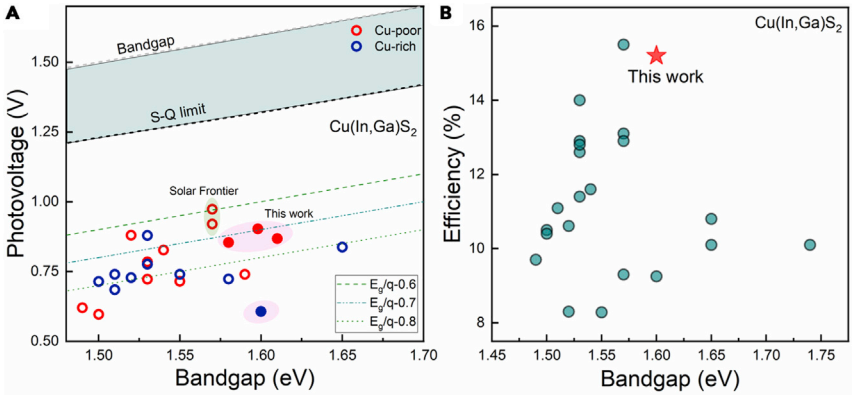

Figure 6. Summary of the photovoltage and efficiency in context to literature

(A and B) (A) Photovoltage (V_{oc}) versus band gap (E_g) and (B) efficiency versus band gap (E_g) plot for sulfide solar cells reported in the literature[5,6,9,13–16,29,53,66–72,73] and in this work (shown in filled circles and shaded color). E_g is determined from EQE plots (see Figure S4).

Increasing the carrier concentration in Cu-poor Cu(In,Ga)S_2 through acceptor doping could lead to further improvement. One promising route in this direction could be the alkali-metal treatment, which has proven to be effective in increasing doping concentration and quality in Cu(In,Ga)Se_2 solar cells.[74,75]

In summary, we show the role of Cu content and its relationship with the bulk and interface recombination in Ga containing sulfide chalcopyrite solar cells. By combining optoelectronic analysis with theoretical calculations, we conclude that the Cu_{In}/Cu_{Ga} antisite defects are among the major causes of high bulk recombination in Cu(In,Ga)S_2. We show that composition engineering, particularly in the Cu-poor domain, provides a promising solution to manipulate these performance-limiting defects. We show that—(1) with increased Cu deficiency, deep defects are strongly suppressed, resulting in an increase in QFLS and also in the device V_{oc}, (2) Cu-poor Cu(In,Ga)S_2 is highly compensated with a low carrier concentration of $\sim 3 \times 10^{15}$ cm^{-3} and exhibits drastically longer carrier lifetime,whereas Cu-rich has a much higher carrier concentration of $\sim 1 \times 10^{17}$ cm^{-3} and lower carrier lifetime, and (3) suppression of interface recombination in Zn(O,S) buffer layer Cu-poor devices but not in Cu-rich devices. Tuning the properties in the Cu-poor regime gives excellent absorbers with high QFLS and carrier lifetime, leading to PCE above 15% with a high V_{oc} of 902 mV. The main factors that lead to this efficiency boost are:

(1) Reduction of bulk recombination centers by using Cu-poor and Ga containing absorbers, as evidenced by the increased carrier lifetime.
(2) Reduction of interface recombination by the use of Cu-poor absorbers, which do not require etching, as evidenced by the massively reduced difference between QFLS and open-circuit voltage.
(3) Further reduction of interface recombination by using a buffer with a suitably high conduction band edge, as evidenced by the higher open-circuit voltage obtained with the Zn(O,S) buffer, as compared with CdS buffer.
(4) Likely the reduction of back surface recombination by a Ga gradient by comparison with similar results in the selenide compounds.

In this way, we show improvement not only in the bulk but also interface losses. These results have important implications on the fundamental understanding of defect physics in pure sulfide Cu(In,Ga)S_2. This work addresses a major performance bottleneck for sulfide-based, and particularly, wide-band-gap Cu(In,Ga)S_2 absorber. The V_{oc} deficit in

wide-band-gap Cu(In,Ga)S_2 can be further reduced by improving the bulk quality through post-deposition treatments and optimizing the deposition process, thus offering encouraging prospects for environmentally friendly H_2S-free, Cd-free, and KCN-free solar cells with efficiency approaching 20%, making them suitable for tandem solar cells.

SUPPLEMENTAL INFORMATION

Supplemental information can be found online at https://doi.org/10.1016/j.joule.2021.05.004.

EXPERIMENTAL PROCEDURES

Resource availability

Lead contact

Further information and requests for resources and materials should be directed to and will be fulfilled by the lead contact, Sudhanshu Shukla (sudhanshu.shukla@uni.lu)

Materials availability

This study did not generate new unique materials.

Data and code availability

The published article includes all data analyzed and necessary to draw the conclusions of this study in the figures and tables of the main text or supplemental information. Further information and requests for further data should be directed to the lead contact.

ACKNOWLEDGMENTS

The authors acknowledge Dr. Nathalie Valle and Dr. Brahime El Adib, Luxembourg Institute for Science and Technology (LIST), for SIMS measurement. M.S. and D.A. gratefully acknowledge partial funding of this research through the Luxembourgish Fond National de la Recherche FNR through the MASSENA project (FNR PRIDE/15/10935404). CL studies were supported by the EPSRC under grant number EP/R025193/1. Dr. Christian Monachon of Attolight is thanked for his ongoing support of the CL system. D.D. was financially supported by the Conseil de l'Action Internationale (CAI) through a doctorate grant "Coopération au Développment". We acknowledge access to various computational resources: the Tier-1 supercomputer of the Fédération Wallonie-Bruxelles funded by the Walloon Region (grant agreement no. 1117545) and all the facilities provided by the Université Catholique de Louvain (CISM/UCL) and by the Consortium des Equipements de Calcul Intensif en Fédération Wallonie-Bruxelles (CECI).

AUTHOR CONTRIBUTIONS

S. Shukla, M.S., and S. Siebentritt conceived the idea and designed experiments. S. Shukla wrote the first draft of the manuscript, and S. Siebentritt supervised the project. S. Shukla prepared the samples and performed structural characterizations. M.S. and M.M. contributed to device fabrication. M.S. performed and analyzed electrical measurements. D.A. and S. Shukla performed and analyzed PL measurements. S.P., G.K., and R.O. performed and analyzed CL measurements. D.D., G.-M.R., and G.H. performed *ab initio* calculations. G.K., G.H., R.O., and S. Siebentritt participated in the discussion of the data and writing of the manuscript.

DECLARATION OF INTERESTS

The authors declare no competing interests.

Received: February 14, 2021
Revised: April 4, 2021
Accepted: May 4, 2021
Published: June 7, 2021

REFERENCES

1. Albrecht, S., and Rech, B. (2017). Perovskite solar cells: on top of commercial photovoltaics. Nat. Energy *2*, 16196.

2. Jošt, M., Kegelmann, L., Korte, L., and Albrecht, S. (2020). Monolithic perovskite tandem solar cells: a review of the present status and advanced characterization methods toward 30% efficiency. Adv. Energy Mater. *10*, 1904102.

3. Al-Ashouri, A., Köhnen, E., Li, B., Magomedov, A., Hempel, H., Caprioglio, P., Márquez, J.A., Morales Vilches, A.B., Kasparavicius, E., Smith, J.A., et al. (2020). Monolithic perovskite/silicon tandem solar cell with >29% efficiency by enhanced hole extraction. Science *370*, 1300–1309.

4. Zafoschnig, L.A., Nold, S., and Goldschmidt, J.C. (2020). The race for lowest costs of electricity production: techno-economic analysis of silicon, perovskite and tandem solar cells. IEEE J. Photovoltaics *10*, 1632–1641.

5. Lomuscio, A., Rödel, T., Schwarz, T., Gault, B., Melchiorre, M., Raabe, D., and Siebentritt, S. (2019). Quasi-fermi-level splitting of Cu-poor and Cu-rich CuInS2 absorber layers. Phys. Rev. Applied *11*, 054052.

6. Hiroi, H., Iwata, Y., Adachi, S., Sugimoto, H., and Yamada, A. (2016). New World-record efficiency for pure-sulfide Cu(in,Ga)S2 thin-film solar cell With Cd-free buffer layer via KCN-free process. IEEE J. Photovoltaics *6*, 760–763.

7. Kim, S., Nagai, T., Tampo, H., Ishizuka, S., and Shibata, H. (2020). Large open-circuit voltage boosting of pure sulfide chalcopyrite Cu(In,Ga)S2 prepared using Cu-deficient metal precursors. Prog. Photovolt. Res. Appl. *28*, 816–822.

8. Kaigawa, R., Funahashi, K., Fujie, R., Wada, T., Merdes, S., Caballero, R., and Klenk, R. (2010). Tandem solar cells with Cu(In,Ga)S2 top cells on ZnO coated substrates. Sol. Energy Mater. Sol. Cells *94*, 1880–1883.

9. Lewerenz, H.J., Goslowsky, H., Husemann, K.-D., and Fiechter, S. (1986). Efficient solar energy conversion with CuInS2. Nature *321*, 687–688.

10. Nakamura, M., Yamaguchi, K., Kimoto, Y., Yasaki, Y., Kato, T., and Sugimoto, H. (2019). Cd-free Cu(In,Ga)(Se,S)2 thin-film solar cell with record efficiency of 23.35%. IEEE J. Photovoltaics *9*, 1863–1867.

11. NREL (2020). Best research-cell efficiency chart. https://www.nrel.gov/pv/cell-efficiency.html.

12. Shockey-Queisser limit for single junction solar cell under AM 1.5 G spectrum is calculated using principle of detailed balance of absorption and emission of radiation, assuming creation of one e-h pair/photon and only radiative recombination.

13. Merdes, S., Mainz, R., Klaer, J., Meeder, A., Rodriguez-Alvarez, H., Schock, H.W., Lux-Steiner, M.C., and Klenk, R. (2011). 12.6% efficient CdS/Cu(In,Ga)S2-based solar cell with an open circuit voltage of 879mV prepared by a rapid thermal process. Sol. Energy Mater. Sol. Cells *95*, 864–869.

14. Hiroi, H., Iwata, Y., Sugimoto, H., and Yamada, A. (2016). Progress toward 1000-mV open-circuit voltage on chalcopyrite solar cells. IEEE J. Photovoltaics *6*, 1630–1634.

15. Barange, N., Chu, V.B., Nam, M., Ahn, I.-H., Kim, Y.D., Han, I.K., Min, B.K., and Ko, D.-H. (2016). Ordered nanoscale heterojunction architecture for enhanced solution-based CuInGaS2 thin film solar cell performance. Adv. Energy Mater. *6*, 1601114.

16. He, G., Yan, C., Li, J., Yuan, X., Sun, K., Huang, J., Sun, H., He, M., Zhang, Y., Stride, J.A., et al. (2020). 11.6% efficient pure sulfide Cu(In,Ga)S2 solar cell through a Cu-deficient and KCN-free process. ACS Appl. Energy Mater. *3*, 11974–11980.

17. Scheer, R. (2012). Open questions after 20 years of CuInS2 research. Prog. Photovolt.: Res. Appl. *20*, 507–511.

18. Chen, H., Wang, C.-Y., Wang, J.-T., Hu, X.-P., and Zhou, S.-X. (2012). First-principles study of point defects in solar cell semiconductor CuInS2. J. Appl. Phys. *112*, 084513.

19. Lomuscio, A., Sood, M., Melchiorre, M., and Siebentritt, S. (2020). Phonon coupling and shallow defects in CuInS2. Phys. Rev. B *101*, 085119.

20. Binsma, J.J.M., Giling, L.J., and Bloem, J. (1982). Luminescence of CuInS2: I. J. Lumin. *27*, 35–53.

21. Hofhuis, J., Schoonman, J., and Goossens, A. (2008). Elucidation of the excited-state dynamics in CuInS2 thin films. J. Phys. Chem. C *112*, 15052–15059.

22. Thomere, A., Guillot-Deudon, C., Caldes, M.T., Bodeux, R., Barreau, N., Jobic, S., and Lafond, A. (2018). Chemical crystallographic investigation on Cu2S-In2S3-Ga2S3 ternary system. Thin Solid Films *665*, 46–50.

23. Elanzeery, H., Melchiorre, M., Sood, M., Babbe, F., Werner, F., Brammertz, G., and Siebentritt, S. (2019). Challenge in Cu-rich CuInSe2 thin film solar cells: defect caused by etching. Phys. Rev. Materials *3*, 055403.

24. Ghorbani, E., Erhart, P., and Albe, K. (2019). Energy level alignment of Cu(In,Ga)(S,Se)2 absorber compounds with In2S3, NaIn5S8, and CuIn5S8 Cd-free buffer materials. Phys. Rev. Materials *3*, 075401.

25. Weinhardt, L., Fuchs, O., Groß, D., Storch, G., Umbach, E., Dhere, N.G., Kadam, A.A., Kulkarni, S.S., and Heske, C. (2005). Band alignment at the CdS/Cu(In,Ga)S2 interface in thin-film solar cells. Appl. Phys. Lett. *86*, 062109.

26. Hengel, I., Neisser, A., Klenk, R., and Lux-Steiner, M.C. (2000). Current transport in CuInS2:Ga/Cds/Zno – solar cells. Thin Solid Films *361–362*, 458–462.

27. Klenk, R. (2001). Characterisation and modelling of chalcopyrite solar cells. Thin Solid Films *387*, 135–140.

28. Unold, T., Sieber, I., and Ellmer, K. (2006). Efficient CuInS2 solar cells by reactive magnetron sputtering. Appl. Phys. Lett. *88*, 213502.

29. Merdes, S., Sáez-Araoz, R., Ennaoui, A., Klaer, J., Lux-Steiner, M.C., and Klenk, R. (2009). Recombination mechanisms in highly efficient thin film Zn(S,O)/Cu(In,Ga)S2 based solar cells. Appl. Phys. Lett. *95*, 213502.

30. Konovalov, I. (2004). Material requirements for CIS solar cells. Thin Solid Films *451–452*, 413–419.

31. Wilhelm, H., Schock, H.-W., and Scheer, R. (2011). Interface recombination in heterojunction solar cells: influence of buffer layer thickness. J. Appl. Phys. *109*, 084514.

32. Neisser, A., Hengel, I., Klenk, R., Matthes, T.W., Álvarez-García, J., Pérez-Rodríguez, A., Romano-Rodríguez, A., and Lux-Steiner, M.-C. (2001). Effect of Ga incorporation in sequentially prepared CuInS2 thin film absorbers. Sol. Energy Mater. Sol. Cells *67*, 97–104.

33. Gloeckler, M., and Sites, J.R. (2005). Efficiency limitations for wide-band-gap chalcopyrite solar cells. Thin Solid Films *480–481*, 241–245.

34. Merdes, S., Abou-Ras, D., Mainz, R., Klenk, R., Lux-Steiner, M.C., Meeder, A., Schock, H.W., and Klaer, J. (2013). CdS/Cu(In,Ga)S2 based solar cells with efficiencies reaching 12.9% prepared by a rapid thermal process. Prog. Photovolt.: Res. Appl. *21*, 88–93.

35. Klenk, R., Bakehe, S., Kaigawa, R., Neisser, A., Reiß, J., and Lux-Steiner, M.C. (2004). Optimising the open-circuit voltage of Cu(In,Ga)S2 solar cells—design and analysis. Thin Solid Films *451–452*, 424–429.

36. Riedel, I., Riediger, J., Ohland, J., Keller, J., Knipper, M., Parisi, J., Mainz, R., and Merdes, S. (2011). Photoelectric characterization of Cu(In,Ga)S2 solar cells obtained from rapid thermal processing at different temperatures. Sol. Energy Mater. Sol. Cells *95*, 270–273.

37. Scheer, R., Klenk, R., Klaer, J., and Luck, I. (2004). CuInS2 based thin film photovoltaics. Sol. Energy *77*, 777–784.

38. Scheer, R., Walter, T., Schock, H.W., Fearheiley, M.L., and Lewerenz, H.J. (1993). CuInS2 based thin film solar cell with 10.2% efficiency. Appl. Phys. Lett. *63*, 3294–3296.

39. Marsen, B., Wilhelm, H., Steinkopf, L., Klemz, S., Unold, T., Scheer, R., and Schock, H.-W. (2011). Effect of copper-deficiency on multi-stage co-evaporated Cu(In,Ga)S2 absorber layers and solar cells. Thin Solid Films *519*, 7224–7227.

40. Ennaoui, A., Bär, M., Klaer, J., Kropp, T., Sáez-Araoz, R., and Lux-Steiner, M.C. (2006). Highly-efficient Cd-free CuInS2 thin-film solar cells and mini-modules with Zn(S,O) buffer layers prepared by an alternative chemical bath process. Prog. Photovolt.: Res. Appl. *14*, 499–511.

41. Gabor, A.M., Tuttle, J.R., Bode, M.H., Franz, A., Tennant, A.L., Contreras, M.A., Noufi, R., Jensen, D.G., and Hermann, A.M. (1996). Band-gap engineering in Cu(In,Ga) Se2 thin films grown from (In,Ga)2Se3 precursors. Sol. Energy Mater. Sol. Cells *41–42*, 247–260, 247–260.

42. Feurer, T., Bissig, B., Weiss, T.P., Carron, R., Avancini, E., Löckinger, J., Buecheler, S., and

Tiwari, A.N. (2018). Single-graded CIGS with narrow bandgap for tandem solar cells. Sci. Technol. Adv. Mater. *19*, 263–270.

43. Schock, H.W., and Scheer, R. (2011). Thin film heterostructures. In Chalcogenide Photovoltaics (Wiley-VCH Verlag), pp. 9–127.

44. Chirilă, A., Buecheler, S., Pianezzi, F., Bloesch, P., Gretener, C., Uhl, A.R., Fella, C., Kranz, L., Perrenoud, J., Seyrling, S., et al. (2011). Highly efficient Cu(In,Ga)Se2 solar cells grown on flexible polymer films. Nat. Mater. *10*, 857–861.

45. Gabor, A.M., Tuttle, J.R., Albin, D.S., Contreras, M.A., Noufi, R., and Hermann, A.M. (1994). High-efficiency CuInxGa1−xSe2 solar cells made from (Inx,Ga1−x)2Se3 precursor films. Appl. Phys. Lett. *65*, 198–200.

46. Wurfel, P. (1982). The chemical potential of radiation. J. Phys. C: Solid State Phys. *15*, 3967–3985.

47. Gütay, L., and Bauer, G.H. (2009). Local fluctuations of absorber properties of Cu(In,Ga)Se2 by sub-micron resolved PL towards "real life" conditions. Thin Solid Films *517*, 2222–2225.

48. Babbe, F., Choubrac, L., and Siebentritt, S. (2018). The optical diode ideality factor enables fast screening of semiconductors for solar cells. Sol. RRL *2*, 1800248.

49. Kirchartz, T., Márquez, J.A., Stolterfoht, M., and Unold, T. (2020). Photoluminescence-based characterization of halide perovskites for photovoltaics. Adv. Energy Mater. *10*, 1904134.

50. Levin, I. (2018). NIST Inorganic Crystal Structure Database (ICSD) (National Institute of Standards and Technology). https://doi.org/10.18434/M32147.

51. Schwarz, T., Lomuscio, A., Siebentritt, S., and Gault, B. (2020). On the chemistry of grain boundaries in CuInS2 films. Nano Energy *76*, 105081.

52. Fiechter, S., Tomm, Y., Kanis, M., Scheer, R., and Kautek, W. (2008). On the homogeneity region, growth modes and optoelectronic properties of chalcopyrite-type CuInS2. phys. stat. sol. (b) *245*, 1761–1771.

53. Kaigawa, R., Neisser, A., Klenk, R., and Lux-Steiner, M.-C. (2002). Improved performance of thin film solar cells based on Cu(In,Ga)S2. Thin Solid Films *415*, 266–271.

54. Klenk, R., Walter, T., Schmid, D., and Schock, H.W. (1993). Growth mechanisms and diffusion in multinary and multilayer chalcopyrite thin films. Jpn. J. Appl. Phys. *32*, 57.

55. Wolter, M.H., Bissig, B., Avancini, E., Carron, R., Buecheler, S., Jackson, P., and Siebentritt, S. (2018). Influence of sodium and rubidium postdeposition treatment on the quasi-fermi level splitting of Cu(In,Ga)Se2 thin films. IEEE J. Photovoltaics *8*, 1320–1325.

56. Babbe, F., Choubrac, L., and Siebentritt, S. (2016). Quasi Fermi level splitting of Cu-rich and Cu-poor Cu(In,Ga)Se2 absorber layers. Appl. Phys. Lett. *109*, 082105.

57. Abou-Ras, D., Koch, C.T., Küstner, V., van Aken, P.A., Jahn, U., Contreras, M.A., Caballero, R., Kaufmann, C.A., Scheer, R., Unold, T., and Schock, H.-W. (2009). Grain-boundary types in chalcopyrite-type thin films and their correlations with film texture and electrical properties. Thin Solid Films *517*, 2545–2549.

58. Zhang, S.B., Wei, S.-H., Zunger, A., and Katayama-Yoshida, H. (1998). Defect physics of the CuInSe2 chalcopyrite semiconductor. Phys. Rev. B *57*, 9642–9656.

59. Leach, A.D.P., Shen, X., Faust, A., Cleveland, M.C., La Croix, A.D., Banin, U., Pantelides, S.T., and Macdonald, J.E. (2016). Defect luminescence from wurtzite CuInS2 nanocrystals: combined experimental and theoretical analysis. J. Phys. Chem. C *120*, 5207–5212.

60. Sood, M., Elanzeery, H., Adeleye, D., Lomuscio, A., Werner, F., Ehre, F., Melchiorre, M., and Siebentritt, S. (2020). Absorber composition: a critical parameter for the effectiveness of heat treatments in chalcopyrite solar cells. Prog. Photovolt. Res. Appl. *28*, 1063–1076.

61. Moore, J.E., Dongaonkar, S., Chavali, R.V.K., Alam, M.A., and Lundstrom, M.S. (2014). Correlation of built-in potential and I–V crossover in thin-film solar cells. IEEE J. Photovoltaics *4*, 1138–1148.

62. Werner, F., Wolter, M.H., Siebentritt, S., Sozzi, G., Di Napoli, S., Menozzi, R., Jackson, P., Witte, W., Carron, R., Avancini, E., et al. (2018). Alkali treatments of Cu(In,Ga)Se2 thin-film absorbers and their impact on transport barriers. Prog. Photovolt. Res. Appl. *26*, 911–923.

63. Sozzi, G., Napoli, S.D., Menozzi, R., Werner, F., Siebentritt, S., Jackson, P., et al. (2017). Influence of conduction band offsets at window/buffer and buffer/absorber interfaces on the Roll-Over of J-V curves of CIGS solar cells. 44th Photovolt. Specialist Conference (PVSC) (IEEE Publications), pp. 2205–2208.

64. Siebentritt, S. (2016). Basics of Chalcogenide Thin Film Solar Cell, Photovoltaic Solar Energy: From Fundamentals to Applications (John Wiley & Sons).

65. Larsson, F., Nilsson, N.S., Keller, J., Frisk, C., Kosyak, V., Edoff, M., and Törndahl, T. (2017). Record 1.0 V open-circuit voltage in wide band gap chalcopyrite solar cells. Record. Prog. Photovolt.: Res. Appl. *25*, 755–763.

66. Scheer, R., Alt, M., Luck, I., and Lewerenz, H.J. (1997). Electrical properties of coevaporated CuInS2 thin films. Sol. Energy Mater. Sol. Cells *49*, 423–430.

67. Walter, T., Braunger, D., Dittrich, H., Köble, C., Herberholz, R., and Schock, H.W. (1996). Sequential processes for the deposition of polycrystalline Cu(In,Ga)(S,Se)2 thin films: growth mechanism and devices. Sol. Energy Mater. Sol. Cells *41–42*, 355–372.

68. Klenk, R., Blieske, U., Dieterle, V., Ellmer, K., Fiechter, S., Hengel, I., Jäger-Waldau, A., Kampschulte, T., Kaufmann, C., Klaer, J., et al. (1997). Properties of CuInS2 thin films grown by a two-step process without H2S. Sol. Energy Mater. Sol. Cells *49*, 349–356.

69. Siemer, K., Klaer, J., Luck, I., Bruns, J., Klenk, R., and Bräunig, D. (2001). Efficient CuInS2 solar cells from a rapid thermal process (RTP). Sol. Energy Mater. Sol. Cells *67*, 159–166.

70. Watanabe, T., Nakazawa, H., and Matsui, M. (1998). Improvement of the electrical properties of Cu-poor CuInS2 thin films by sodium incorporation. Jpn. J. Appl. Phys. *37*, L1370–L1372.

71. Ohashi, T., Hashimoto, Y., and Ito, K. (1999). Cu(In1-xGax)S2 thin-film solar cells with efficiency above 12%, fabricated by sulfurization. Jpn. J. Appl. Phys. *38*, L748–L750.

72. Mainz, R., Streicher, F., Abou-Ras, D., Sadewasser, S., Klenk, R., and Lux-Steiner, M.C. (2009). Combined analysis of spatially resolved electronic structure and composition on a cross-section of a thin film Cu(In1–x Gax)S2 solar cell. phys. stat. sol. (a) *206*, 1017–1020.

73. Klenk, R., Klaer, J., Köble, C., Mainz, R., Merdes, S., Rodriguez-Alvarez, H., Scheer, R., and Schock, H.W. (2011). Development of CuInS2-based solar cells and modules. Sol. Energy Mater. Sol. Cells *95*, 1441–1445.

74. Yuan, Z.-K., Chen, S., Xie, Y., Park, J.-S., Xiang, H., Gong, X.-G., and Wei, S.-H. (2016). Na-diffusion enhanced p-type conductivity in Cu(In,Ga)Se2: a new mechanism for efficient doping in semiconductors. Adv. Energy Mater. *6*, 1601191.

75. Siebentritt, S., Avancini, E., Bär, M., Bombsch, J., Bourgeois, E., Buecheler, S., Carron, R., Castro, C., Duguay, S., Félix, R., et al. (2020). Heavy alkali treatment of cu(in,ga)se2 solar cells: surface versus bulk effects. Adv. Energy Mater. *10*, 1903752.